AMPK and AKT protein kinases hierarchically phosphorylate the N-terminus of the FOXO1 transcription factor, modulating interactions with 14-3-3 proteins

Received for publication, March 28, 2019, and in revised form, July 10, 2019 Published, Papers in Press, July 15, 2019, DOI 10.1074/jbc.RA119.008649

Maria Saline[‡1,2,3], **Lukas Badertscher**[‡1,4], **Madita Wolter**[§], **Roxanne Lau**[§], **Anders Gunnarsson**[‡], **Tomas Jacso**[‡3,5], **Tyrrell Norris**[‡], **Christian Ottmann**[§], **and Arjan Snijder**[‡6]

From [‡]*Discovery Biology, Discovery Sciences, R&D, AstraZeneca, Gothenburg, Sweden, the* [§]*Laboratory of Chemical Biology, Department of Biomedical Engineering and Institute for Complex Molecular Systems, Eindhoven University of Technology, P. O. Box 513, 5600 MB Eindhoven, The Netherlands*

Edited by Wolfgang Peti

Forkhead box protein O1 (FOXO1) is a transcription factor involved in various cellular processes such as glucose metabolism, development, stress resistance, and tumor suppression. FOXO1's transcriptional activity is controlled by different environmental cues through a myriad of posttranslational modifications. In response to growth factors, the serine/threonine kinase AKT phosphorylates Thr^{24} and Ser^{256} in FOXO1 to stimulate binding of 14-3-3 proteins, causing FOXO1 inactivation. In contrast, low nutrient and energy levels induce FOXO1 activity. AMP-activated protein kinase (AMPK), a master regulator of cellular energy homeostasis, partly mediates this effect through phosphorylation of Ser^{383} and Thr^{649} in FOXO1. In this study, we identified Ser^{22} as an additional AMPK phosphorylation site in FOXO1's N terminus, with Ser^{22} phosphorylation preventing binding of 14-3-3 proteins. The crystal structure of a FOXO1 peptide in complex with 14-3-3 σ at 2.3 Å resolution revealed that this is a consequence of both steric hindrance and electrostatic repulsion. Furthermore, we found that AMPK-mediated Ser^{22} phosphorylation impairs Thr^{24} phosphorylation by AKT in a hierarchical manner. Thus, numerous mechanisms maintain FOXO1 activity via AMPK signaling. AMPK-mediated Ser^{22} phosphorylation directly and indirectly averts binding of 14-3-3 proteins, whereas phosphorylation of Ser^{383} and Thr^{649} complementarily stimulates FOXO1 activity. Our results shed light on a mechanism that integrates inputs from both AMPK and AKT signaling pathways in a small motif to fine-tune FOXO1 transcriptional activity.

The forkhead box O (FOXO)[7] family of transcription factors is well-conserved throughout evolution, and they control the expression of a multitude of genes involved in various cellular processes. FOXO1 (FKHR), one of the family members, has been shown to regulate cellular homeostasis, insulin and glucose metabolism, immune responses, cell cycle progression, apoptosis, and senescence (1). Moreover, FOXO1-null mice are not able to complete embryonic development, confirming its essential role (2).

The transcriptional activity of FOXO1 is tightly regulated through numerous posttranslational modifications, such as phosphorylation, methylation, acetylation, ubiquitination, and glycosylation (reviewed in Refs. 3, 4). Multiple kinases are known to reduce FOXO1 activity via phosphorylation (*e.g.* AKT (5); CDK5 (6), PKA (7), CDK2 (8), CDK1 (9), and DYRK1, GSK3, and CK1 (10)). Of these, FOXO1 phosphorylation by the PI3K/AKT pathway is extensively studied. In response to a range of extracellular stimuli like growth factors, insulin, and cytokines, AKT phosphorylates Thr^{24}, Ser^{256}, and Ser^{319} in FOXO1 (11, 12). This allows binding of 14-3-3 scaffolding proteins to FOXO1 and consequent inhibition of transcriptional activity through export from the nucleus to the cytoplasm. 14-3-3 proteins are ubiquitously expressed in mammalian cells, and they mainly regulate the function of binding partners by affecting their subcellular localization (13). Notably, a triple mutant of FOXO1 (T24A/S256A/S319A), which cannot be phosphorylated by AKT, is predominantly nuclear and constitutively active because interactions with 14-3-3 proteins are abolished (14).

In contrast, various kinases activate the transcriptional activity of FOXO1 (AMPK (15), MST1 (16), and extracellular signal-regulated kinase and p38 (17)). AMP-activated protein kinase (AMPK) is a major regulator of cellular energy homeostasis and is activated under conditions such as nutrient deprivation or oxidative stress (18–22). Yun *et al.* (15) showed that AMPK

L. B., A. G., T. N., and A. S. are employees and shareholders of AstraZeneca. T. J. is an employee and shareholder of Nuevolution.

This article contains Figs. S1–S9.

The atomic coordinates and structure factors (codes 6QZR and 6QZS) have been deposited in the Protein Data Bank (http://wwpdb.org/).

The NMR data reported in this paper have been submitted to the BMRB under accession numbers 27336 (NTDΔ), 27337 (NTDΔ-pSer^{22}), and 27320 (NTDΔ-pThr^{24}).

[1] Both authors contributed equally to this work.

[2] Present address: Chalmers University of Technology, 412 96 Gothenburg, Sweden.

[3] Previous fellow of the AstraZeneca postdoctoral program.

[4] Fellow of the AstraZeneca postdoctoral program.

[5] Present address: Nuevolution A/S, Rønnegade 8, 2100 Copenhagen, Denmark.

[6] To whom correspondence should be addressed. Tel.: 46-317763691; E-mail: arjan.snijder@astrazeneca.com.

[7] The abbreviations used are: FOXO, forkhead box O; FKHR, forkhead in rhabdomyosarcoma; AMPK, AMP-activated protein kinase; FHD, forkhead box domain; TAD, transcription activation domain; NTD, N-terminal domain; SSP, secondary structure propensity; SPR, surface plasmon resonance; TCEP, tris(2-carboxyethyl)phosphine; HMQC, Heteronuclear Multiple Quantum Coherence; RU, resonance units; SOFAST-HMQC, Selective Optimized Flip-Angle Short-Transient heteronuclear multiple quantum coherence.

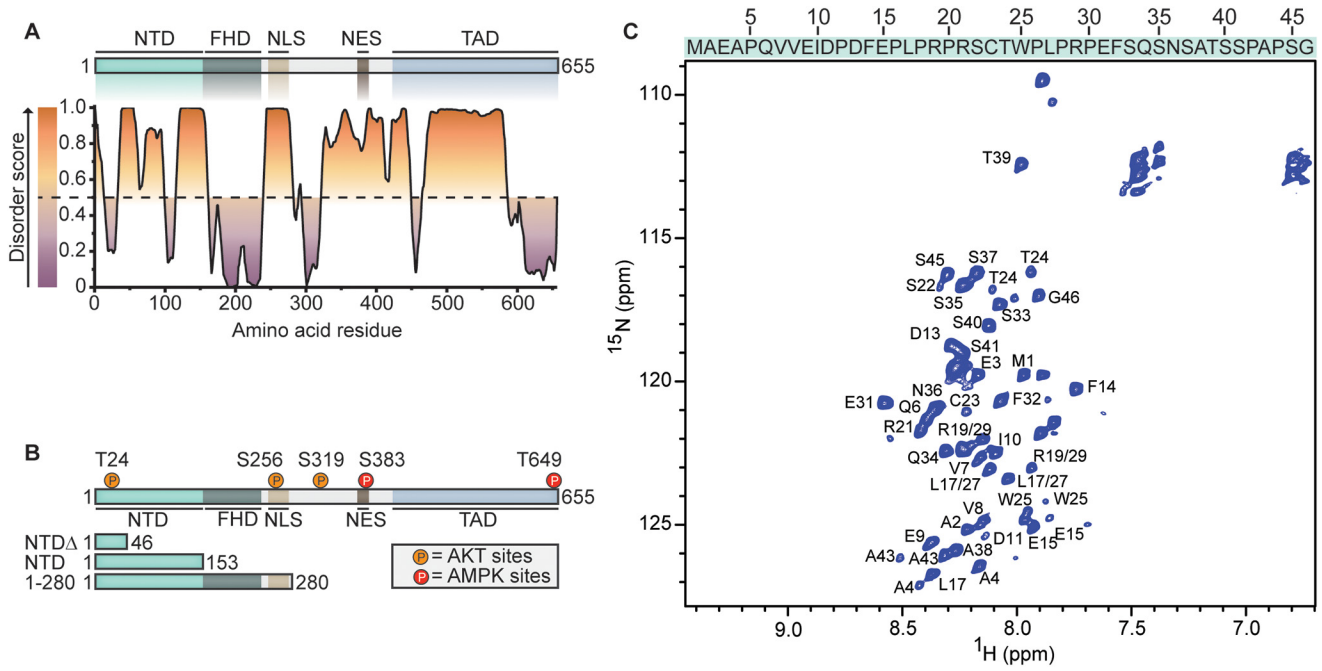

Figure 1. Analysis of intrinsically disordered regions in FOXO1. *A*, representation of the functional domains of FOXO1: NTD 1–153, FHD 154–244, TAD 421–655. A disorder score was predicted for each amino acid using PONDR-FIT (23). The *dashed line* at 0.5 of the *y* axis separates residues that were predicted to be disordered (score > 0.5, *orange*) and ordered (score < 0.5, *purple*). *B*, the known AKT and AMPK phosphorylation sites in FOXO1 are highlighted in *orange* and *red*, respectively. Constructs that were used in this study are indicated: NTDΔ (1–46), NTD (1–153), and a fragment containing the NTD, FHD, and nuclear localization signal (1–280), which was used to analyze interactions with 14-3-3 proteins in cells (Fig. 4*A*). *C*, assignment of the ^{1}H-^{15}N HMQC spectrum of NTDΔ. Several amino acids display pairs of signals, as these are preceded by prolines that occur in both *cis* and *trans* conformation. Amino acids Leu^{17}/Leu^{27} and Arg^{19}/Arg^{29} could not be distinguished because they are flanked by prolines, which do not show signals in a ^{1}H-^{15}N HMQC spectrum. Residues of the purification tag were observed but were not assigned. Amino acid sequence of NTDΔ is indicated on top of the NMR spectrum in one-letter code.

phosphorylates FOXO1 on residues Ser^{383} and Thr^{649}; however, the molecular mechanism for increased FOXO1 activity upon phosphorylation of these residues remains elusive. Moreover, the authors suggested that additional AMPK sites might exist that could further explain the regulation of the transcriptional activity of FOXO1 by AMPK.

In this work, we identified Ser^{22} in FOXO1 as an additional AMPK phosphorylation site. Structural and biophysical data elucidated that phosphorylation of Ser^{22} reduces binding of 14-3-3 proteins to FOXO1 through steric hindrance and electrostatic repulsion. At the same time, Ser^{22} phosphorylation indirectly prevented 14-3-3 binding by negatively regulating Thr^{24} phosphorylation by AKT. Interestingly, phosphorylation of Thr^{24} did not affect phosphorylation of Ser^{22} by AMPK to a similar extent, suggesting hierarchical cross-talk between both signaling pathways. Ser^{22} phosphorylation both directly and indirectly abrogates complex formation with 14-3-3 proteins and plays a central role in controlling the transcriptional activity of FOXO1.

Results

The N-terminal domain of FOXO1 is intrinsically disordered

The FOXO1 protein consists of three major functional domains: the Forkhead box domain (FHD), which is responsible for DNA binding; the C-terminal transcription activation domain (TAD); and the less characterized N-terminal domain (NTD). Moreover, the protein contains signals that mediate nuclear localization and nuclear export (Fig. 1*A*). Although the FHD and TAD have been extensively studied, little is known about the contribution of the NTD regarding transcriptional activity of FOXO1.

To better understand the structural features of the different domains of FOXO1, we first performed *in silico* predictions of the disorder tendency (23, 24). This analysis suggested a folded FHD (154–244) that is flanked by predominantly disordered regions (disorder scores ≥ 0.5, Fig. 1*A*). Of note, crystal structures have been solved for the FOXO1 FHD (25, 26), confirming a structured organization of this region. Next, we focused on the NTD and purified two recombinant proteins for structural examination using 2D NMR. One protein encompassed the full NTD (1–153) and the other a N-terminal region of the NTD (1–46), hereafter referred to as NTD and NTDΔ, respectively (Fig. 1*B*). The ^{1}H-^{15}N Heteronuclear Single Quantum Coherence (HSQC) NMR spectra of NTDΔ (Fig. 1*C*) and the NTD (Fig. S1) showed narrow dispersions of ^{1}H-^{15}N chemical shifts in the ^{1}H dimension (7.7–8.6 ppm), a characteristic of proteins lacking secondary structure elements. Although backbone resonances of NTDΔ were fully assigned, individual assignments of amino acids in the entire NTD could not be obtained because of peak overlaps. Nevertheless, both spectra showed a high similarity in chemical shifts and line widths, indicating an intrinsically disordered nature of the NTD. A secondary structure propensity (SSP) analysis (27) further confirmed a predominantly random coil conformation of NTDΔ based on the Cα and Cβ chemical shifts from the 3D ^{13}C-^{15}N HNCαCβ experiment (Fig. S2). However, residues 21–25 and 35–40 had positive average SSP scores, 0.19 and 0.08, respectively, suggesting a weak partial α-helical propensity of those regions.

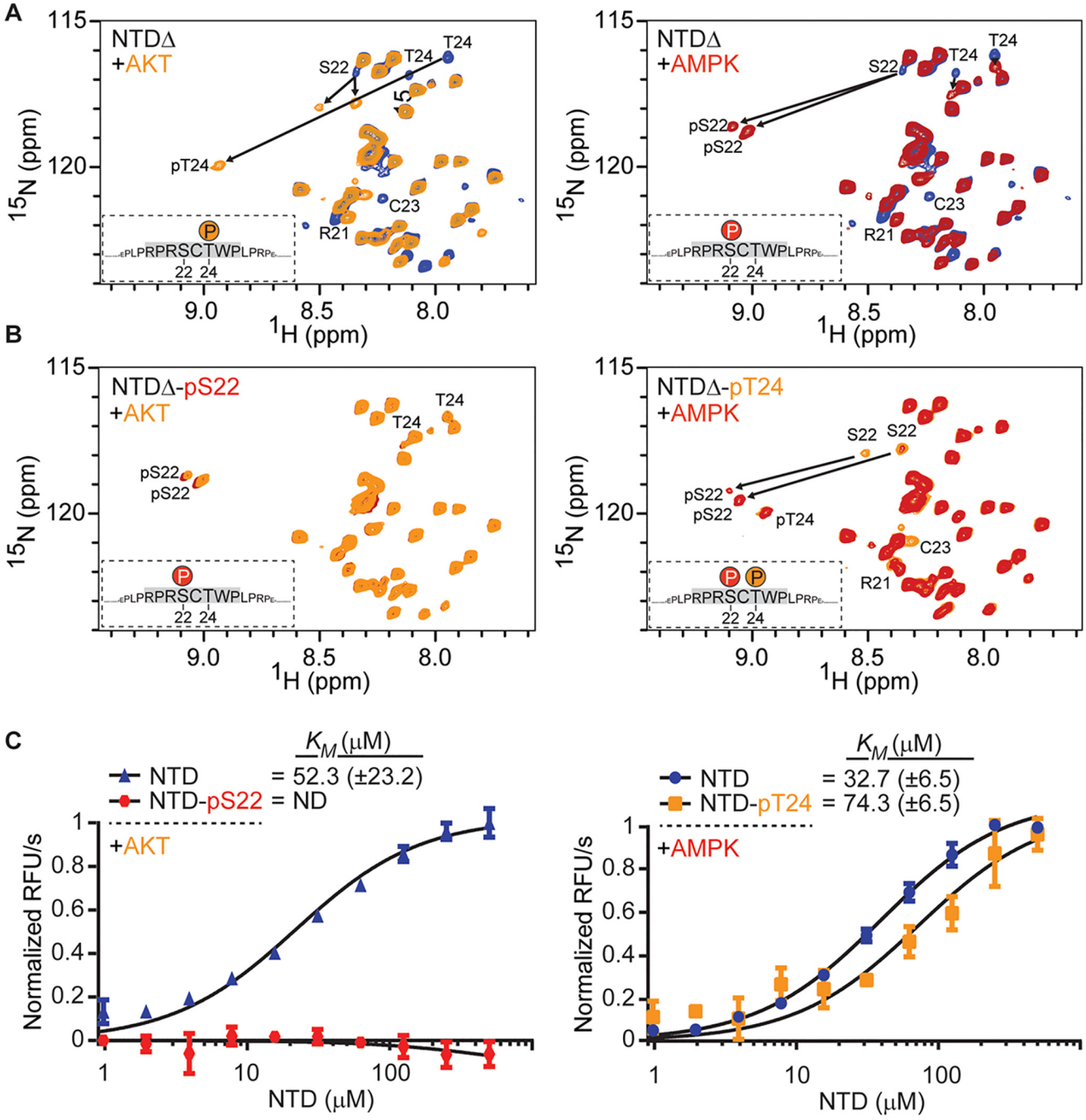

Figure 2. Phosphorylation of the NTD by AKT and AMPK. *A*, 2D ^{1}H-^{15}N HMQC NMR spectra of NTDΔ incubated for 3 h with purified AKT (*orange*) or AMPK (*red*) to assess Thr^{24} and Ser^{22} phosphorylation by AKT and AMPK, respectively. Chemical shift changes of phosphorylated amino acids are indicated by *arrows*. Doubling of peaks for pSer^{22} suggests dual conformations. *B*, 2D ^{1}H-^{15}N HMQC NMR spectra of prephosphorylated NTDΔ incubated with the indicated kinases for 4.5 h; NTDΔ-pSer^{22} with AKT to monitor Thr^{24} phosphorylation (*orange*) and NTDΔ-pT24 with AMPK to analyze Ser^{22} phosphorylation (*red*). Chemical shift changes of phosphorylated amino acids are indicated by *arrows*. *C*, the activities of both AKT and AMPK kinases on different substrates were analyzed using a fluorescence-based ADP biosensor. The unphosphorylated NTD as substrate for AKT and AMPK is shown in *blue*. The activity of AKT on NTD-pSer^{22} is shown in *red*. The activity of AMPK on NTD-pThr^{24} is shown in *orange*. K_m values were determined based on the initial reaction rates. Data are mean ± S.D. from three independent experiments. *ND*, not detectable.

The NTD retains unstructured properties upon Thr^{24} phosphorylation by AKT

The NTD of FOXO1 contains one of the two 14-3-3 binding motifs (amino acids 19–26), and phosphorylation of Thr^{24} by AKT is required to mediate interactions with 14-3-3 proteins. Interestingly, residues 21–25 showed a weak α-helical propensity (Fig. S2), and, therefore, we hypothesized that phosphorylation of Thr^{24} might induce structural changes that could influence 14-3-3 binding.

To measure phosphorylation of Thr^{24} in time-resolved 2D ^{1}H-^{15}N Heteronuclear Multiple Quantum Coherence (HMQC) NMR experiments, either NTDΔ or the full NTD were incubated with purified AKT. Over the course of 3 h, a single chemical shift appeared at 8.95/119.89 (^{1}H/^{15}N) ppm (Fig. 2*A*,

Fig. S3*A*), a region typical for phosphorylated residues (28). Simultaneously, two chemical shifts assigned to Thr^{24} gradually disappeared from 7.97/116.45 (^{1}H/^{15}N) and 8.13/116.82 (^{1}H/^{15}N) ppm, highlighting strong phosphorylation of Thr^{24} by AKT, as expected. The appearance of two distinct individual chemical shifts might be caused by specific *cis* and *trans* conformations of the flanking proline residue, as observed with other intrinsically disordered proteins (29). NTDΔ contains 10 prolines, and the presence of 15 Hα/N peaks in a ^{15}N-^{13}C Hα(Cα)N NMR spectra revealed that five prolines occur in both *cis* and *trans* conformations (Fig. S4). Apart from the changes in chemical shifts for Thr^{24}, only minor differences were detected for residues in proximity to the phosphorylation site: Leu^{17}/Leu^{27}, Arg^{19}/Arg^{29}, Arg^{21}, Ser^{22}, Cys^{23}, and Tyr^{25}.

Finally, the SSP scores for both the unphosphorylated and Thr^{24} phosphorylated NTDΔ were comparable (Fig. S2). This suggested that Thr^{24} phosphorylation by AKT does not influence the local structural organization of the NTD.

AMPK phosphorylates Ser^{22} in the NTD

AMPK has been shown to phosphorylate Ser^{383} and Thr^{649} in FOXO1, but it was suspected that additional AMPK phosphorylation sites might exist (30). Several AMPK phosphorylation motifs have been described (15, 22, 31, 32), and central elements are two to three basic and/or hydrophobic residues at position 3–7 N-terminally together with one hydrophobic residue at position 3–4 C-terminally of the phosphorylated residue. Interestingly, Ser^{22} in the NTD of FOXO1 fulfills these criteria and was predicted by the PhosphoNET software (33) as a potential AMPK site.

To analyze whether AMPK can phosphorylate Ser^{22} *in vitro*, we first performed an LC-MS measurement and identified one major and one minor phosphorylation site by the occurrence of a +80-Da and +160-Da peak. Subsequent peptide digestion and LC-MS/MS suggested Ser^{22} as an AMPK phosphorylation site in the NTD of FOXO1 (Fig. S5).

To confirm phosphorylation of Ser^{22} by AMPK, we incubated NTDΔ as well as the full NTD with purified AMPK and evaluated the chemical shifts in time-resolved 2D ^{1}H-^{15}N HMQC NMR experiments. Within 2 h, gradual disappearance of the Ser^{22} chemical shift at 8.36/116.64 (^{1}H/^{15}N) ppm was observed in combination with the emergence of two new peaks at 9.04/118.80 (^{1}H/^{15}N) ppm and 9.09/118.65 (^{1}H/^{15}N) ppm, indicating that Ser^{22} was phosphorylated by AMPK (Fig. 2*A* and Fig. S3*A*). Flanking residues next to the phosphorylation site were shifted in the NMR spectra (Leu^{17}/Leu^{27}, Arg^{19}/Arg^{29}, Arg^{21}, Cys^{23}, Thr^{24}, and Tyr^{25}), as observed for the phosphorylation of Thr^{24} by AKT within the same region. There was no substantial difference between the SSP scores of the unphosphorylated and Ser^{22}-phosphorylated NTDΔ (Fig. S2). Hence, neither Ser^{22} nor Thr^{24} phosphorylation changed the secondary structure of this region of the NTD.

Phosphorylation of Ser^{22} by AMPK decreases phosphorylation of Thr^{24} by AKT

The proximity of Ser^{22} and Thr^{24} led us explore whether the phosphorylation status of one of those residues affects the subsequent phosphorylation of the other site or whether phosphorylation occurs independently. Time-resolved 2D NMR experiments on the prephosphorylated NTDΔ were conducted. NTDΔ-pThr^{24} was incubated with purified AMPK, and over the course of 4.5 h, two peaks assigned to Ser^{22} at 8.53/117.87 (^{1}H/^{15}N) ppm and 8.37/117.71 (^{1}H/^{15}N) ppm disappeared (Fig. 2*B*, *red*). In parallel, two new peaks appeared at 9.07/119.49 (^{1}H/^{15}N) ppm and 9.11/119.14 (^{1}H/^{15}N) ppm, illustrating successful phosphorylation of Ser^{22}. Full phosphorylation of Ser^{22} in NTDΔ-pThr^{24} was achieved after about 4.5 h, approximately twice the time compared with the unphosphorylated protein as a substrate. Next, we incubated NTDΔ-pSer^{22} with AKT. No peaks were shifted in the NMR spectra after 4.5 h, highlighting that AKT was unable to phosphorylate Thr^{24} within this time scale (Fig. 2*B*, *orange*). After 24 h, a weak signal appeared for pThr^{24}, with a concomitant decrease in intensity of the Thr^{24} peak, suggesting very weak phosphorylation by AKT (data not shown). Comparable results were observed with the full NTD (Fig. S3*B*). Taken together, the prior phosphorylation status of Ser^{22} drastically affected subsequent phosphorylation of Thr^{24} by AKT, but pThr^{24} only moderately reduced the phosphorylation rate of Ser^{22} by AMPK.

To further substantiate this observation, Michaelis–Menten kinetics (K_m) were determined for AMPK and AKT with the unphosphorylated and prephosphorylated NTD. For AMPK, the K_m of the unphosphorylated NTD and NTD-pThr^{24} as a substrate was 32 μM and 74 μM, respectively (Fig. 2*C*, *right panel*). This statistically significant ($p = 0.0016$) 2.3-fold increase of K_m was in a similar range as observed in the NMR measurements. For AKT, the K_m was 52 μM for the unphosphorylated NTD, whereas the K_m could not be determined for the NTD-pSer^{22}, implying that it is a poor AKT substrate (Fig. 2*C*, *left panel*). Overall, time-resolved 2D NMR measurements combined with the biochemical assay demonstrate a hierarchical order where the AMPK-mediated phosphorylation of Ser^{22} in the NTD has a strong regulatory effect on Thr^{24} phosphorylation by AKT but not vice versa.

Phosphorylation of Ser^{22} prevents interactions of FOXO1 with 14-3-3 proteins

A major mechanism to control FOXO1 transcriptional activity is the binding of 14-3-3 proteins. Different 14-3-3 interaction motifs have been described in the literature, and FOXO1 contains two mode I motifs, R*XX*(pS/pT)*X*P (34). A prerequisite for complex formation is phosphorylation of one residue in each of the 14-3-3 interaction motifs by AKT: Thr^{24} and Ser^{256} (11). Interestingly, Ser^{22} is located in the N-terminal 14-3-3 binding interface (Fig. S8*B*). To examine the impact of Ser^{22} phosphorylation on 14-3-3 binding, we first studied the interaction of the NTD and 14-3-3 proteins *in vitro* using surface plasmon resonance (SPR) direct binding assays. 14-3-3 ζ was immobilized to the SPR sensor surface, and binding affinities of the unphosphorylated NTD or the NTD phosphorylated on Ser^{22}, Thr^{24}, or both were measured. As expected, an AKT-phosphorylated NTD (pThr^{24}) caused a strong interaction with 14-3-3 ζ (K_d, 5.1 μM), confirming the central role of pThr^{24} as binding platform for

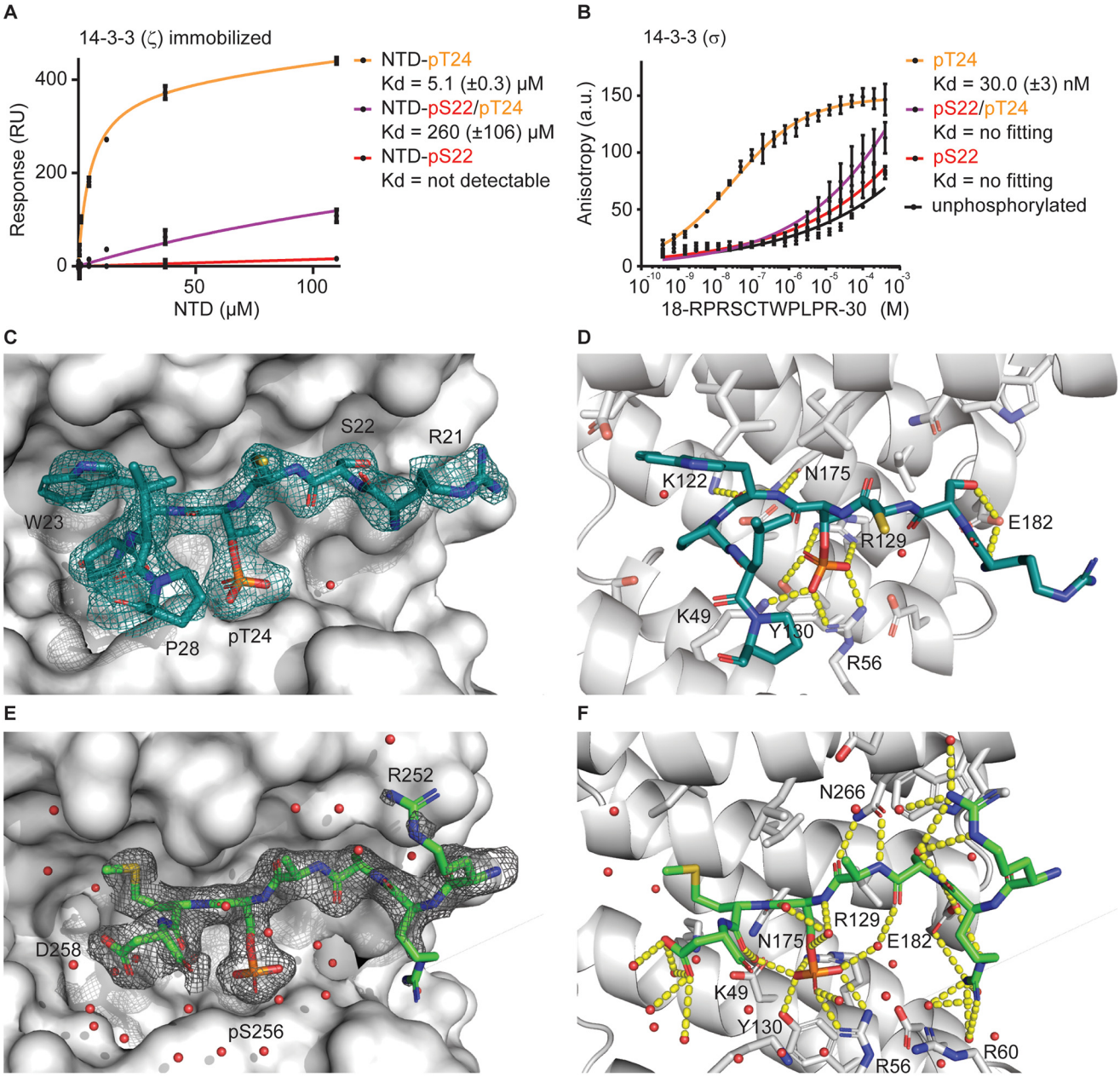

Figure 3. Phosphorylation of Ser[22] in the NTD of FOXO1 hinders 14-3-3 interactions *in vitro*. *A*, surface plasmon resonance binding analysis of 14-3-3 ζ and the NTD of FOXO1 phosphorylated at the indicated residues. NTD-pThr[24] served as positive control, and the unphosphorylated NTD was used as a linear component for data correction. Data are expressed as mean ± S.D. of technical triplicates from one representative experiment. *B*, fluorescence anisotropy binding analysis of interactions between 14-3-3 σ and the FOXO1 peptide ([18]RPRSCTWPLPR[30]) in different phosphorylation states. Data are expressed as means ± S.D. from three independent experiments and fitted with Prism (specific binding with the Hill slope). *C*, representative FOXO1/14-3-3 complex with displayed electron density (final 2Fo-Fc, contoured at 1σ) with 14-3-3 as a *gray surface*, FOXO1-pThr[24] as *sticks*, and water as a *red sphere*. Amino acids of the FOXO1-pThr[24] peptide are indicated in one-letter code. *D*, details of the interactions between FOXO1-pThr[24] and 14-3-3 σ. Amino acids of 14-3-3 σ are indicated in one-letter code, and hydrogen bonds are illustrated by *yellow dashed lines*. *E*, FOXO1-pSer[256]/14-3-3 complex with displayed electron density (Final 2Fo-Fc, contoured at 1σ) with 14-3-3 as a *gray surface*, FOXO1-pSer[256] as *sticks*, and water as a *red sphere*. Amino acids of the FOXO1-pSer[256] peptide are indicated in one-letter code. *F*, details of the interactions between FOXO1-pSer[256] and 14-3-3 σ. Amino acids of 14-3-3 σ are indicated in one-letter code, and hydrogen bonds are illustrated by *yellow dashed lines*.

14-3-3 proteins (Fig. 3*A*). An AMPK-phosphorylated NTD (pSer[22]) showed a very weak affinity to 14-3-3 ζ. Interestingly, the double-phosphorylated NTD (pSer[22]/pThr[24]) also possessed a reduced affinity for 14-3-3 ζ of more than 50-fold (K_d, 260 μM). Similar results were observed with the θ isoform of 14-3-3 (Fig. S6*A*), and it appeared that phosphorylation of Ser[22] strongly blocked 14-3-3 binding even in the context of phosphorylated Thr[24].

Crystal structures of pThr[24] and pSer[256] peptides in complex with 14-3-3 σ

To fully understand the consequence of Ser[22] phosphorylation on 14-3-3 binding, we aimed to crystallize the interface of the NTD and 14-3-3. However, no crystals could be obtained with the full NTD, and, therefore, peptides were used to represent the different phosphorylated 14-3-3 recognition sites of

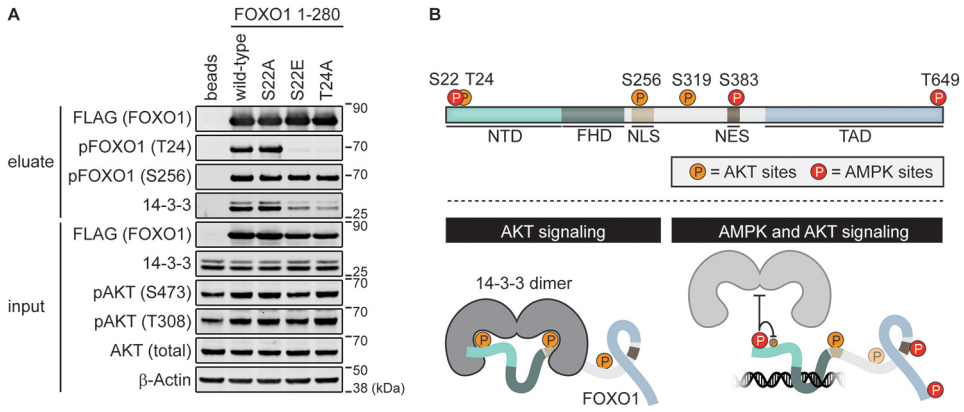

Figure 4. The phosphorylation state of Ser[22] regulates binding of 14-3-3 proteins to FOXO1 in HEK293 cells. *A*, FLAG-FOXO1(1–280)–EGFP fusion proteins were expressed in HEK293 cells for 20 h. After cell lysis, complexes were immunoprecipitated using anti-FLAG-agarose beads and analyzed by Western blotting with the indicated antibodies. Eluates were adjusted according to amounts of bait proteins (anti-FLAG). The T24A construct served as a positive control for a reduced 14-3-3 interaction. The activity of AKT kinase was monitored with pAKT (Ser[473]/Thr[308]) antibodies. *B*, schematic overview of the regulation of transcriptional activity of FOXO1 by the AKT and AMPK signaling pathways. Optimal growth conditions result in active AKT, and phosphorylation of Thr[24] as well as Ser[256] in FOXO1 stimulates binding of 14-3-3 proteins to inhibit its transcriptional activity. On the other hand, phosphorylation of Ser[22] by AMPK is likely to increase the activity of FOXO1 by preventing 14-3-3 binding both directly through steric hindrance and electrostatic repulsion and indirectly by attenuating Thr[24] phosphorylation by AKT.

FOXO1. The peptide representing the pThr[24] site consists of 11 amino acids with the sequence [18]RPRSCTWPLPR[30].

First, Fluorescein amidite (FAM)-labeled versions of the peptides in different phosphorylation states were used in fluorescence anisotropy measurements to test whether they reflect the binding behavior between the NTD and 14-3-3 proteins observed in SPR experiments. The highest affinity was measured between 14-3-3 σ and the pThr[24] peptide (30 nM), whereas the pSer[22] and double-phosphorylated peptides had weaker binding affinities (Fig. 3*B*). For 14-3-3 ζ, the pThr[24] peptide had an affinity of 18.3 nM, whereas the double-phosphorylated peptide had a binding affinity of 12.9 μM (Fig. S6*B*). Moreover, the binding of the pSer[22] and unphosphorylated peptide could not be quantified. Together, these results are in line with the findings of the SPR experiments employing the entire NTD.

Next, unlabeled peptides were used for structure analysis. The pThr[24] peptide in complex with 14-3-3 σ produced crystals of the space group $P2_1$ that diffracted to 2.3 Å and harbored eight 14-3-3/peptide molecules in the asymmetric unit (Fig. S7*A*). Up to nine residues of the 11 amino acids comprising the pThr[24] peptide could be built into the electron density (Fig. 3*C*). The peptide binds into the amphipathic groove of the 14-3-3 protein, where the side chain of Trp[25] establishes an extensive hydrophobic contact with the "hydrophobic roof" (35) of the 14-3-3 monomer binding channel. The two prolines (Pro[26] and P28) induce a strong turn in the peptide, guiding the chain away from the Trp[25] position toward the 14-3-3 dimer interface and out of the central binding channel. The pThr[24] is coordinated by Lys[49], Arg[57], Arg[129], and Tyr[130] of the protein. Additional polar contacts were mainly established via the peptide backbone and polar residues of 14-3-3 (carbonyl of Trp[25] with Lys[122], nitrogen of Trp[25] with Asn[175], and nitrogen of Arg[21] with Glu[182]) (Fig. 3*D*). Interestingly, the hydroxyl group of Ser[22] forms a polar contact with Glu[182], locking this residue in all eight monomers in a similar conformation (Fig. S7*A*). A close-up of that conformation explains how a phosphorylation of this residues disrupts the binding of the double-phosphorylated peptide and the NTD. The serine fills a flat pocket of the 14-3-3 surface; any extension of that residue will cause a steric clash with the protein and impair binding.

To complete the picture of FOXO1 binding to 14-3-3, the structure was also solved of the complex between pSer[256] and the C-terminal 14-3-3 binding site to 1.9 Å and in the space group $P2_12_12_1$, with two molecules found in the asymmetric unit (Fig. S7*C*). Seven residues (Arg[252]-Asp[258]) of the 12 amino acids comprising the FOXO1-pSer[256] peptide ([251]RRRAASMDNNSK[262]) could be built into the electron density (Fig. 3*E*). The phosphorylated serine (pSer[256]) is found in the same pocket as pThr[24], coordinated by Arg[57], Arg[129], and Tyr[130] of 14-3-3 (Fig. 3*F*). The hydrophobic roof of the 14-3-3 monomer binding channel is occupied by the side chain of Met[257], whereas residues Asp[258] and Asn[259] extend out of the binding groove. The small side chain of the x-2 residue, Ala[254], is in a similar position as the corresponding residue Ser[22]; however, it lacks the opportunity to engage in a polar contact with Glu[182] in 14-3-3. These results emphasize a distinct feature of the N-terminal 14-3-3 binding site, where interactions can be directly regulated through phosphorylation of both Thr[24] and Ser[22].

Ser[22] phosphorylation hinders 14-3-3 interactions in cells

To further investigate the significance of Ser[22] and Thr[24] phosphorylation regarding 14-3-3 interactions in a cellular context, we used FOXO1 (1–280) constructs (Fig. 1*B*) bearing either phosphodeficient (S22A and T24A) or phosphomimetic (S22E) mutations for immunoprecipitation in HEK293 cells. Amino acids 1–280 of FOXO1 contained both 14-3-3 interaction motifs, but it was observed that a single point mutation (T24A) in the N-terminal binding site is sufficient to strongly reduce the overall 14-3-3 interactions because of loss of avidity (13). The WT construct was phosphorylated on Thr[24] and precipitated, as expected, various isoforms of 14-3-3 proteins (Fig. 4*A*). Phosphorylation of Thr[24] was a consequence of continuous AKT activity under optimal growth conditions, confirmed with pAKT antibodies (Thr[308] and Ser[473]). For our experi-

ments, we selected a HEK293 cell line with low endogenous FOXO1 levels; therefore, we could ensure that the signal of the pFOXO1 (Thr^{24}) antibody represented the phosphorylation status of the ectopically expressed proteins. The T24A mutation that prevented phosphorylation by AKT strongly reduced 14-3-3 interactions, as described previously (13, 36). The S22E mutation reflected an intracellular state of continuous AMPK activity, where Ser^{22} is phosphorylated, and strikingly showed attenuated 14-3-3 binding comparable with the T24A mutation. The structural data propose that mimicking the Ser^{22} phosphorylation directly prevents 14-3-3 binding through steric hindrance and electrostatic repulsion in the binding pocket. Moreover, despite active AKT, Thr^{24} phosphorylation was not detectable, and it seemed that Ser^{22} phosphorylation additionally controls 14-3-3 binding indirectly by preventing AKT from accessing its phosphorylation site. This is consistent with our *in vitro* data showing that NTD-pSer^{22} is a poor AKT substrate. Overall, our results substantiate the central role of the phosphorylation state of Ser^{22} to control binding of 14-3-3 proteins, thus regulating the transcriptional activity of FOXO1.

Discussion

FOXO transcription factors orchestrate the expression of genes involved in central cellular processes such as apoptosis, cell cycle progression, and stress resistance. Among the plethora of posttranslational modifications that regulate FOXO1 transcriptional activity, phosphorylation by AKT and the energy-sensing AMPK act in an opposing fashion. AKT-mediated phosphorylation of FOXO1 induces binding of 14-3-3 proteins, its nuclear export, and consequent transcriptional inactivation (13), whereas phosphorylation by AMPK has been shown to increase FOXO1 activity (37). In this work, we expand the interaction network of AKT and AMPK on FOXO1 by demonstrating that AMPK can phosphorylate the NTD of FOXO1 on Ser^{22} to affect 14-3-3 interactions.

Attenuated binding of 14-3-3 proteins to FOXO1, caused by phosphorylation of Ser^{22}, could be explained by conformational changes within the NTD of FOXO1, steric and electrostatic effects decreasing the binding affinity between FOXO1 and 14-3-3, or a reduction in AKT-mediated phosphorylation of Thr^{24} in FOXO1.

Conformational switching driven by posttranslational modification of intrinsically disordered proteins has been shown, for example, for Nucleophosmin (NPM1), where successive multiple phosphorylations induce a change from an ordered pentamer to a disordered monomeric state to control its function (30). Another example includes 4EBP2, where phosphorylation by ERK2 induces a conformational change from a disordered to a folded structure to form a regulatory switch (38). Our NMR results showed that no conformational changes occur in the NTD of FOXO1 by Ser^{22} or Thr^{24} phosphorylation and exclude this as a probable cause to modulate 14-3-3 binding.

Another possibility could be that phosphorylation of Ser^{22} indirectly prevents 14-3-3 interactions by diminishing Thr^{24} phosphorylation by AKT. In a cellular context, we observed that AKT was unable to phosphorylate Thr^{24} in the phosphomimetic S22E FOXO1, whereas the phosphodeficient S22A as well as WT FOXO1 were unaffected. Moreover, time-resolved 2D NMR and measuring the Michaelis–Menten kinetics also showed that pSer^{22} impedes Thr^{24} phosphorylation by AKT. Interestingly, the crystal structure of AKT with bound substrate (39) suggests that a phosphoserine in the −2 position of the AKT phosphorylation site would be unfavorable electrostatically, leading to steric hindrance and obstructing binding of AKT. A similar sensitivity to mutations in the AKT binding motif was observed in patients with diffuse large B cell lymphoma (36). It was shown that the presence of point mutations at Arg^{19} and Arg^{21} in the NTD of FOXO1 diminished phosphorylation of Thr^{24} by AKT, as we observed for pSer^{22}. Together, this emphasizes that phosphorylation of Ser^{22} renders the NTD a poor substrate for AKT and diminishes Thr^{24} phosphorylation. This, in turn, will reduce 14-3-3 interactions and activate FOXO1.

Besides the effect on phosphorylation of Thr^{24} by AKT, we observed that phosphorylation of Ser^{22} directly reduces the affinity for the ζ and θ isoforms of 14-3-3 in SPR measurements. Our structure of 14-3-3 σ and a pT24 FOXO1 peptide further showed that phosphorylation of Ser^{22} at the −2 position of the canonically phosphorylated serine or threonine in the 14-3-3 motif would lead to both electrostatic repulsion and steric hindrance. Comparable alleviation of 14-3-3 binding through phosphorylation at the same position within the binding surface has been reported previously for RGS18 (40) and kinesin-14 (41). The effect of steric hindrance at the −2 position is additionally illustrated by a mutation in C-Raf, where a mutation of serine to a leucine (S257L) reduces 14-3-3 binding (42). Together, the phosphorylation status of Ser^{22} will translate into regulatory effects on 14-3-3 binding through steric and electrostatic forces in the binding pocket.

A sequence alignment of the human FOXO proteins shows full conservation of the serine corresponding to Ser^{22} in FOXO1 within the N-terminal 14-3-3 recognition motif (Fig. S8*B*). This offers the possibility that other FOXO family members might be subjected to a similar modulation of 14-3-3 binding through phosphorylation of the conserved serine. However, the kinases involved could vary between different FOXO family members because of sequence differences in the proximity of the phosphorylation site. AMPK is capable to recognize promiscuous substrates, but a hydrophobic residue N-terminal of its phosphorylation site is a core feature in the recognition motif. Strikingly, this hydrophobic residue in position −7 (Leu^{17} in FOXO1) is only present in FOXO1, whereas FOXO3, FOXO4, and FOXO6 have a polar glutamine residue in the corresponding position that is likely to prevent AMPK binding (Fig. S8*B*). In fact, upon inhibition of AMPK, decreased transcriptional activity of FOXO1 was observed, whereas the activity of FOXO3 was unaffected (19). Whether AKT-mediated binding of 14-3-3 proteins can be modified through cross-talk between diverse kinases in different FOXO proteins awaits further analysis. The key components of both PI3K/AKT and AMPK signaling pathways are well-conserved throughout evolution. Interestingly, sequence alignments of different FOXO1 homologs between various species suggest that the additional regulation of 14-3-3 binding by AMPK might have evolved in vertebrates, as indicated by a conserved AMPK recognition motif. In *Drosophila melanogaster*, two residues of the AMPK recognition motif are substituted with amino acids that contain

different chemical properties. This makes it unlikely that dFoxO is subjected to a comparable regulation by AMPK. Finally, the direct impairment of 14-3-3 binding through phosphorylation at the −2 position by specific kinases may be a general regulation mechanism among 14-3-3 substrates because a bioinformatic analysis revealed a serine as the most prevalent residue at this position (34).

AMPK and AKT pathways are heavily intertwined by negative feedback loops. This makes it challenging to quantify the specific contribution of Ser^{22} phosphorylation regarding FOXO1 regulation in a cellular context. Furthermore, interpretation of data and literature is complicated, as tool compounds used to influence AMPK activity (*i.e.* resveratrol and AICAR) can lead to secondary effects. Cell- and tissue-related differences in signaling pathways, and particularly AMPK and AKT activity, further hamper interpretation of the data. Even though AMPK and AKT act antagonistically on each other and FOXO1, cellular conditions have been described where both kinases are simultaneously active (43–45). Zou *et al.* (45) suggested that metformin activates FOXO1 via AMPK signaling through impeding phosphorylation by AKT and concomitantly increasing its nuclear localization. Although phosphorylation of FOXO1 was only analyzed on Ser^{256} and not Thr^{24} in that study, the mechanism where phosphorylation of Ser^{22} by AMPK leads to loss of 14-3-3 interactions could in part explain the described nuclear retention of FOXO1. Another report described enhanced FOXO1 transcriptional activity after H_2O_2 treatment, which is known to activate AMPK. Paradoxically, the increased transcriptional activity was accompanied by a higher level of AKT-phosphorylated pFOXO1 (46). This could be a consequence of increased AMPK activity under these conditions that might overrule the AKT-mediated export of FOXO1 from the nucleus to the cytoplasm. Although further studies are required to fully understand the observed cross-talk between AMPK and AKT signaling to regulate FOXO1 activity as well as the relevant cellular context, we demonstrate a hierarchy in its kinase regulation. Thereby, AKT and AMPK pathways directly integrate on FOXO1 with the potential to fine-tune its transcriptional activity through interactions with 14-3-3 proteins.

Experimental procedures

Vector construction

FOXO1 constructs were synthesized by GeneArt and codon-optimized for expression in respective host cells. FOXO1 constructs (NTDΔ and NTD) contained an N-terminal 6× His-Asn tag as well as a tobacco etch virus protease cleavage site for purification of recombinant proteins and were cloned into a pET-24 vector. FOXO1 (1–280) constructs (WT, S22A, S22E, and T24A) that were used in cell experiments carried an N-terminal 3×FLAG-tag as well as C-terminal enhanced GFP and were cloned into a pcDNA3.1 vector.

Expression and purification of FOXO1 proteins

NTDΔ and NTD were expressed in *Escherichia coli* BL21 Star (DE3). Terrific broth (TB) medium was supplemented with kanamycin (100 mg/l), 3 mM $MgCl_2$, 0.8% glycerol, 0.02% glucose, and 0.2% lactose for autoinduction (47). The cells were grown at 37 °C for 4 h, followed by 20-h growth at 20 °C before lysis in HEPES buffer (pH 7.4), 150 mM NaCl, 1 mM TCEP, and 1× protease inhibitors (Roche, 26733200) using a cell disruptor at 25 kilopound per square inch (ksi) (Constant Systems). The protein was captured on a HisTrap FF column (GE Healthcare) and subsequently eluted in increasing imidazole concentrations (10–400 mM). The protein was further purified on a size exclusion S75 column (GE Healthcare) that was pre-equilibrated in 20 mM Tris-HCl (pH 7.4), 150 mM NaCl, 1 mM TCEP, and 1× protease inhibitors.

The double-isotopically labeled protein ($^{13}C/^{15}N$) was expressed in *E. coli* BL21 Star (DE3) and grown in TB medium to an optical density of 2. Then cells were harvested by centrifugation at 4500 × *g* for 5 min and resuspended in half of the volume of optimized high cell density minimal medium (48) supplemented with $^{15}NH_4Cl$ (Cambridge Isotope Lab, NLM-467-PK) and ^{13}C glucose (Cambridge Isotope Lab, CLM-1396-PK). After 1 h of adaptation at 37 °C, the temperature was lowered to 20 °C, and protein expression was induced with 0.5 mM isopropyl 1-thio-β-D-galactopyranoside for 16–48 h. Labeled proteins were purified as described above, with exception of the final buffer that was for the NTD (50 mM NaPi (pH 6.8), 120 mM NaCl, 1 mM TCEP, and 10% D_2O) and for NTDΔ (20 mM HEPES (pH 6.7), 100 mM NaCl, 1 mM TCEP, and 10% D_2O).

Peptides

EPLPRPRSCTWPLPRPE, EPLPRPR(pS)CTWPLPRPE (pSer^{22}), and EPLPRPRSC(pT)WPLPRPE (pThr^{24}) were purchased from Cambridge Research Biochemicals and diluted in H_2O. AKT1-PKB-α S473D (amino acids 118–480, referred to as AKT) and 14-3-3 proteins (isoforms θ and ζ) were produced by the Reagents and Services Division of the MRC Protein Phosphorylation and Ubiquitylation Unit of the University of Dundee and stored at −80 °C. AMPK (His_6-α2, S108A-β2, γ1) was expressed and purified as described previously (18) and used at a stock concentration of 6 mg/ml in 120 mM Tris-HCl (pH 8.0), 200 mM NaCl, and 10% glycerol. The ADP biosensor 5-ATR-ParM (tetramethylrhodamine-labeled ParM protein) was expressed, purified, and labeled as described previously (49).

Phosphorylation of FOXO1

The NTD of FOXO1 in 20 mM Tris-HCl (pH 7.4), 150 mM NaCl, 1 mM TCEP, 1× protease inhibitor (Roche, 26733200), and 0.1 mM Na_3VO_4 was supplemented with AKT or AMPK to a final concentration of 0.19 μM and 0.33 μM, respectively. For sequential phosphorylation of FOXO1, AKT was added overnight before the reaction could proceed with AMPK for one additional night at 20 °C. Prior to surface plasmon resonance experiments, the FOXO1 preparations were buffer-exchanged to 10 mM HEPES (pH 7.4), 350 mM NaCl, 1 mM TCEP, and 0.05% (v/v) Tween 20 using a NAP-10 column. Samples were separated with Novex 4–12% BisTris gels (Invitrogen) in 1× MES running buffer, and phosphorylation was assessed by staining with Pro-Q Diamond Phosphoprotein Gel Stain (Invitrogen) followed by SYPRO Ruby Gel Stain (Invitrogen) and Phos-tag gels (Wako Pure Chemical Industries Ltd.) stained with Instant Blue (Expedeon). Further confirmation of phosphorylation was performed by MS, where the molecular mass of

each FOXO1 sample was measured by Electrospray Ionisation-Mass Spectrometry (ESI-MS) micromass ZQ analysis (Waters). Samples were diluted in an equal volume of buffer A (0.1% formic acid and 3% acetonitrile) and separated over a C4 column (Dionex) in a chromatography from 100% buffer A to 100% buffer B (0.1% formic acid and 90% acetonitrile). Mass spectroscopic data were analyzed with the MassLynx software.

Surface plasmon resonance

Experiments were performed on a Biacore 3000 (GE Healthcare) and either 14-3-3 θ or ζ were covalently immobilized on a low-density CM5 chip (Xantec) using standard amine-coupling procedures (1-ethyl-3-(3-dimethylaminopropyl)-carbodiimide (EDC)/N-hydroxysulfosuccinimide (NHS) activation) with proteins in acetate buffer (pH 5.5). The various FOXO1 preparations were injected at a concentration of 330 μM to 17 nM with 10 3× dilution steps. The resonance units (RU) at steady state were recorded, and data were adjusted for nonspecific binding observed with unphosphorylated FOXO1. Steady-state data were fitted to a model with R_{max} fixed at 600 RU or 400 RU for 14-3-3 θ or ζ, respectively, using nonlinear regression in Prism (GraphPad). The kinetic parameters K_{on} and K_{off} of the SPR raw data were extracted using curve fitting in the BiaEvaluation 4.1 software.

NMR

Measurements were recorded on an 800-MHz Bruker Avanze III spectrometer equipped with a cryogenic probe (Bruker) at 20 °C with 330-μl sample in medium-walled tubes. Spectral assignment was obtained by using 2D ^{1}H-^{15}N Selective Optimized Flip-Angle Short-Transient heteronuclear multiple quantum coherence (SOFAST-HMQC) HMQC and a standard Bruker pulse sequence for triple resonance spectra 3D ^{1}H-^{15}N-^{13}C HN$C\alpha C\beta$, HN$C\alpha$, and HNCo$C\alpha C\beta$. All spectra were processed in TopSpin (Bruker), and Collaborative Computational Project for NMR (CCPNMR) (50) was used for sequential assignment of chemical shifts.

To follow the phosphorylation of the NTD by AKT or AMPK, a series of 2D ^{1}H-^{15}N SOFAST HMQC experiments were used for either 100 μM uniformly labeled ^{13}C-^{15}N NTD or 400 μM uniformly labeled ^{13}C-^{15}N NTDΔ. After complete phosphorylation, a 3D HN$C\alpha C\beta$ spectrum was recorded for assignment, followed by addition of the second kinase to obtain the other series of 2D ^{1}H-^{15}N SOFAST HMQC measurements. At completion of the phosphorylation, or after 24 h, a 3D HN$C\alpha C\beta$ spectrum was recorded for assignment of chemical shifts. ^{15}N-^{13}C Hα(Cα)N NMR spectra were recorded to assess conformation of prolines in the NTD, and Hα/N peaks were identified. The integrity of all proteins was monitored by SDS-PAGE after NMR analysis to assure that no proteolytic cleavage occurred during the measurements.

Secondary structure propensity analysis

The secondary chemical shifts ($\Delta\delta$) were calculated as $\Delta\delta = \delta - \delta rc$, where δ is the observed chemical shift, and δrc is the random coil chemical shift (27, 51). The presented SSP score is a weighted average of the $\Delta\delta$ shifts over five residues. Negative SSP values indicate a preference for the β-strand or extended structure, whereas positive values indicate an α-helical propensity. A weighted SSP score of 1 represents a full secondary structure. Prolines as well as residues preceding prolines were excluded from analysis because prolines do not have the backbone amide proton. This makes them invisible in 2D ^{1}H-^{15}N HMQC, and they strongly affect the chemical shifts of flanking residues. The phosphorylated residues are not part of the reference database; hence, a correct comparison could not be made. These residues were excluded from the SSP analysis.

Biochemical enzymatic assay

The ADP-sensing 5-ATR-ParM (49) was used to measure the kinase activity of AKT and AMPK. The assay was carried out in 30 mM Tris-HCl (pH 7.5), 25 mM KCl, and 10 mM $MgCl_2$ buffer supplemented with fresh 1 mM TCEP, 5 μM BSA, and 1× protease inhibitors (Roche, 26733200) on the day of the experiment. FOXO1 peptides were dissolved in H_2O to a concentration of 20 mM. The assay was performed with a total assay volume of 12 μl in a microtiter plate (Greiner, 784900). Under the assay conditions, the biosensor showed a linear response to ADP in the range of 1–400 μM ADP (Ultra-Pure, Promega). First, 0.05 μM 5-ATR-ParM, 1 mM ATP, and varying concentrations of FOXO1 peptide (0.5 mM to 0.25 μM) were diluted in running buffer, centrifuged at 200 × *g* for 1 min, and incubated on ice. After 1 h, enzyme was added as well as AKT (5 nM to 200 nM) for the NTD or NTD-pSer^{22} or AMPK (5 nM to 25 nM) for the NTD or NTD-pThr^{24}. Substrates were pre-equilibrated. The plates were centrifuged at 200 × *g* for 1 min, followed by kinetics measurements. The accumulation of ADP was assessed as an increased fluorescent signal with excitation at 540 nm and an emission filter at 590 nm using a PheraStar microplate reader (BMG Labtech). Data were recorded with an interval of 120 s for 1.5 h and analyzed with the MARS software (BMG Labtech). The initial linear velocity was extracted and plotted against substrate concentration in Prism (GraphPad). The initial velocity was normalized to the maximum initial velocity, except for AKT, with NTD-pSer^{22}. No activity could be measured; therefore, data were scaled using normalization parameters from the measurement of AKT with the NTD. All experiments were performed in triplicate at least three separate times. Data were analyzed using a nonlinear regression Michaelis–Menten model. A K_m for one run in a single experiment (AKT with the NTD, third of four runs) was flagged as an outlier by a Grubb's outlier test and excluded from further analysis. Differences in K_m values were tested for significance with one-way analysis of variance. The K_m shows a significant difference between AMPK with NTD and NTD-pThr^{24} as substrates ($p = 0.0016$); the K_m differences are nonsignificant between AKT NTD and AMPK NTD or NTD-pThr^{24} ($p = 0.0795$ and $p = 0{,}1592$, respectively). The K_m value could not be determined for NTD-pSer^{22} with AKT.

Crystallography

The 14-3-3$\sigma\Delta$C protein (C-terminally truncated 14-3-3 σ, amino acids 1–231) was mixed in a 1:1 ratio with either the FOXO1-pThr^{24} or the FOXO1-pSer^{256} peptide to a final concentration of 12 mg/ml of protein in buffer (20 mM HEPES (pH 7.5), 2 mM $MgCl_2$, and 2 mM β-mercaptoethanol). The 14-3-

3σΔC/FOXO1-pThr[24] mixture was crystallized using the sitting drop method in a 1:1 ratio of 14-3-3σΔC/FOXO1-pThr[24] complex to crystallization buffer (0.1 M BisTris propane (pH 7), 0.2 M sodium nitrate, 28% (v/v) PEG 400, and 5% (w/v) glycerol) and incubated at 4 °C. The 14-3-3σΔC/FOXO1-pSer[256] mixture was crystallized using the sitting drop method in a 1:1 ratio of 14-3-3σΔC/FOXO1-pSer[256] complex to crystallization buffer (0.1 M BisTris propane (pH 7), 0.2 M sodium citrate tribasic dehydrate, 20% (w/v) PEG 3350, and 10% (w/v) glycerol) and incubated at 4 °C.

Diffraction data for the crystals were collected at the synchrotron (PETRA III, Hamburg, Germany) and processed with Diffraction Integration for Advanced Light Sources (DIALS) using xia2. The structures were solved by molecular replacement with a previously solved 14-3-3/peptide complex (PDB code 3MHR), using molrep for the 14-3-3σΔC/FOXO1-pThr[24] structure and Phaser-MR for the 14-3-3σΔC/FOXO1-pSer[256] structure. Model building and refinement of both structures were performed using Coot, REFMAC5, and phenix.refine.

Cell culture and plasmid DNA transfection

HEK293 cells were free of mycoplasma and authenticated by STR DNA profiling analysis. Cells were grown in DMEM (Gibco, 31966) supplemented with 10% FBS (Gibco, 10270-106) without antibiotics at 37 °C in 5% CO_2. Plasmid DNA was transfected with FuGENE HD transfection reagent (Promega) according to the manufacturer's protocol.

FLAG immunoprecipitation

Anti-FLAG M2-agarose affinity gel (A2220) was purchased from Sigma-Aldrich, and immunoprecipitations were performed according to the manufacturer's instructions. In brief, HEK293 cells were transfected in 10-cm dishes with 10 μg of FLAG-tagged fusion proteins. 20 h after transfection, cells were washed with ice-cold PBS and resuspended in 1 ml of lysis buffer (20 mM Tris-HCl (pH 7.4), 150 mM NaCl, 1% Triton X-100 (v/v), 2 mM EDTA, 25 mM NaF, 1 mM Na_3VO_4, 1× cOmplete protease inhibitor mixture (Roche, 26733200)). After incubation on ice for 20 min, lysates were sonicated and cleared by centrifugation (12,000 × *g* for 10 min) before cell extracts were incubated with anti-FLAG M2 beads for 90 min while rotating. Beads were washed with 20 mM Tris-HCl (pH 7.4), 150 mM NaCl and protein complexes were eluted with SDS sample buffer (without DTT). DTT was added to 50 mM final concentration before SDS-PAGE. All steps were performed at 4 °C.

Western blotting and antibodies

Equal amounts of proteins were separated on 4%–12% BisTris gels (Invitrogen) in MES buffer and transferred to nitrocellulose membranes with a Trans-Blot Turbo system (Bio-Rad).

pFOXO1-Thr[24] (9464), pFOXO1-Ser[256] (9461), 14-3-3 (8312), AKT (2938), pAKT-Ser[473] (4060), and pAKT-Thr[308] (13038) antibodies were purchased from Cell Signaling Technology. β-Actin (A1978) and FLAG (F3165) antibodies were from Sigma-Aldrich. IRDye secondary antibodies for Western blotting were from LI-COR, and membranes were scanned using an Odyssey CLx imaging system (LI-COR).

Author contributions—M. S., L. B., T. J., T. N., C. O., and A. S. conceptualization; M. S., L. B., M. W., R. L., A. G., T. J., and A. S. investigation; M. S., L. B., M. W., R. L., and A. S. writing-original draft; A. G., T. J., T. N., and C. O. writing-review and editing; C. O. and A. S. supervision; A. S. funding acquisition.

Acknowledgments—We thank Rachel Rowlinson, Anna Hoyle, and Melanie Snow for help with LC-MS/MS (Discovery Sciences, R&D, AstraZeneca, UK); Puneet Ahuja for NMR setup (Discovery Sciences, R&D, AstraZeneca, Sweden); Mats Ormö for support with the ADP biosensor assay (Discovery Sciences, R&D, AstraZeneca, Sweden); and Ryan Guillbert for providing the ParM protein (Discovery Sciences, R&D, AstraZeneca, UK).

References

1. Martins, R., Lithgow, G. J., and Link, W. (2016) Long live FOXO: unraveling the role of FOXO proteins in aging and longevity. *Aging Cell* **15,** 196–207 CrossRef Medline
2. Hosaka, T., Biggs, W. H., 3rd, Tieu, D., Boyer, A. D., Varki, N. M., Cavenee, W. K., and Arden, K. C. (2004) Disruption of forkhead transcription factor (FOXO) family members in mice reveals their functional diversification. *Proc. Natl. Acad. Sci. U.S.A.* **101,** 2975–2980 CrossRef Medline
3. Klotz, L. O., Sanchez-Ramos, C., Prieto-Arroyo, I., Urbanek, P., Steinbrenner, H., and Monsalve, M. (2015) Redox regulation of FoxO transcription factors. *Redox Biol.* **6,** 51–72 CrossRef Medline
4. Zhao, Y., Wang, Y., and Zhu, W. G. (2011) Applications of post-translational modifications of FoxO family proteins in biological functions. *J. Mol. Cell Biol.* **3,** 276–282 CrossRef Medline
5. Rena, G., Guo, S., Cichy, S. C., Unterman, T. G., and Cohen, P. (1999) Phosphorylation of the transcription factor forkhead family member FKHR by protein kinase B. *J. Biol. Chem.* **274,** 17179–17183 CrossRef Medline
6. Zhou, J., Li, H., Li, X., Zhang, G., Niu, Y., Yuan, Z., Herrup, K., Zhang, Y. W., Bu, G., Xu, H., and Zhang, J. (2015) The roles of Cdk5-mediated subcellular localization of FOXO1 in neuronal death. *J. Neurosci.* **35,** 2624–2635 CrossRef Medline
7. Lee, J. W., Chen, H., Pullikotil, P., and Quon, M. J. (2011) Protein kinase A-α directly phosphorylates FoxO1 in vascular endothelial cells to regulate expression of vascular cellular adhesion molecule-1 mRNA. *J. Biol. Chem.* **286,** 6423–6432 CrossRef Medline
8. Huang, H., Regan, K. M., Lou, Z., Chen, J., and Tindall, D. J. (2006) CDK2-dependent phosphorylation of FOXO1 as an apoptotic response to DNA damage. *Science* **314,** 294–297 CrossRef Medline
9. Yuan, Z., Becker, E. B., Merlo, P., Yamada, T., DiBacco, S., Konishi, Y., Schaefer, E. M., and Bonni, A. (2008) Activation of FOXO1 by Cdk1 in cycling cells and postmitotic neurons. *Science* **319,** 1665–1668 CrossRef Medline
10. Rena, G., Woods, Y. L., Prescott, A. R., Peggie, M., Unterman, T. G., Williams, M. R., and Cohen, P. (2002) Two novel phosphorylation sites on FKHR that are critical for its nuclear exclusion. *EMBO J.* **21,** 2263–2271 CrossRef Medline
11. Brunet, A., Bonni, A., Zigmond, M. J., Lin, M. Z., Juo, P., Hu, L. S., Anderson, M. J., Arden, K. C., Blenis, J., and Greenberg, M. E. (1999) Akt promotes cell survival by phosphorylating and inhibiting a Forkhead transcription factor. *Cell* **96,** 857–868 CrossRef Medline
12. Tang, E. D., Nuñez, G., Barr, F. G., and Guan, K. L. (1999) Negative regulation of the forkhead transcription factor FKHR by Akt. *J. Biol. Chem.* **274,** 16741–16746 CrossRef Medline
13. Rena, G., Prescott, A. R., Guo, S., Cohen, P., and Unterman, T. G. (2001) Roles of the forkhead in rhabdomyosarcoma (FKHR) phosphorylation sites in regulating 14-3-3 binding, transactivation and nuclear targeting. *Biochem. J.* **354,** 605–612 CrossRef Medline
14. Matsuzaki, H., Daitoku, H., Hatta, M., Tanaka, K., and Fukamizu, A. (2003) Insulin-induced phosphorylation of FKHR (Foxo1) targets to proteasomal degradation. *Proc. Natl. Acad. Sci. U.S.A.* **100,** 11285–11290 CrossRef Medline

15. Yun, H., Park, S., Kim, M. J., Yang, W. K., Im, D. U., Yang, K. R., Hong, J., Choe, W., Kang, I., Kim, S. S., and Ha, J. (2014) AMP-activated protein kinase mediates the antioxidant effects of resveratrol through regulation of the transcription factor FoxO1. *FEBS J.* **281,** 4421–4438 CrossRef Medline
16. Yuan, Z., Lehtinen, M. K., Merlo, P., Villén, J., Gygi, S., and Bonni, A. (2009) Regulation of Neuronal Cell Death by MST1-FOXO1 Signaling. *J. Biol. Chem.* **284,** 11285–11292 CrossRef Medline
17. Asada, S., Daitoku, H., Matsuzaki, H., Saito, T., Sudo, T., Mukai, H., Iwashita, S., Kako, K., Kishi, T., Kasuya, Y., and Fukamizu, A. (2007) Mitogen-activated protein kinases, Erk and p38, phosphorylate and regulate Foxo1. *Cell. Signal.* **19,** 519–527 Medline
18. Xiao, B., Sanders, M. J., Carmena, D., Bright, N. J., Haire, L. F., Underwood, E., Patel, B. R., Heath, R. B., Walker, P. A., Hallen, S., Giordanetto, F., Martin, S. R., Carling, D., and Gamblin, S. J. (2013) Structural basis of AMPK regulation by small molecule activators. *Nat. Commun.* **4,** 3017 CrossRef Medline
19. Awad, H., Nolette, N., Hinton, M., and Dakshinamurti, S. (2014) AMPK and FoxO1 regulate catalase expression in hypoxic pulmonary arterial smooth muscle. *Pediatr. Pulmonol.* **49,** 885–897 CrossRef Medline
20. Chen, B. L., Ma, Y. D., Meng, R. S., Xiong, Z. J., Wang, H. N., Zeng, J. Y., Liu, C., and Dong, Y. G. (2010) Activation of AMPK inhibits cardiomyocyte hypertrophy by modulating of the FOXO1/MuRF1 signaling pathway *in vitro*. *Acta Pharmacol. Sin.* **31,** 798–804 CrossRef Medline
21. Lee, K., Ochi, E., Song, H., and Nakazato, K. (2015) Activation of AMP-activated protein kinase induce expression of FoxO1, FoxO3a, and myostatin after exercise-induced muscle damage. *Biochem. Biophys. Res. Commun.* **466,** 289–294 Medline
22. Greer, E. L., Dowlatshahi, D., Banko, M. R., Villen, J., Hoang, K., Blanchard, D., Gygi, S. P., and Brunet, A. (2007) An AMPK-FOXO pathway mediates longevity induced by a novel method of dietary restriction in *C. elegans*. *Curr. Biol.* **17,** 1646–1656 CrossRef Medline
23. Xue, B., Dunbrack, R. L., Williams, R. W., Dunker, A. K., and Uversky, V. N. (2010) PONDR-FIT: a meta-predictor of intrinsically disordered amino acids. *Biochim. Biophys. Acta* **1804,** 996–1010 CrossRef Medline
24. Obradovic, Z., Peng, K., Vucetic, S., Radivojac, P., Brown, C. J., and Dunker, A. K. (2003) Predicting intrinsic disorder from amino acid sequence. *Proteins* **53,** 566–572 CrossRef Medline
25. Brent, M. M., Anand, R., and Marmorstein, R. (2008) Structural basis for DNA recognition by FoxO1 and its regulation by posttranslational modification. *Structure* **16,** 1407–1416 CrossRef Medline
26. Singh, P., Han, E. H., Endrizzi, J. A., O'Brien, R. M., and Chi, Y.-I. (2017) Crystal structures reveal a new and novel FoxO1 binding site within the human glucose-6-phosphatase catalytic subunit 1 gene promoter. *J. Struct. Biol.* **198,** 54–64 CrossRef Medline
27. Marsh, J. A., Singh, V. K., Jia, Z., and Forman-Kay, J. D. (2006) Sensitivity of secondary structure propensities to sequence differences between α- and γ-synuclein: implications for fibrillation. *Protein Sci.* **15,** 2795–2804 CrossRef Medline
28. Selenko, P., Frueh, D. P., Elsaesser, S. J., Haas, W., Gygi, S. P., and Wagner, G. (2008) *In situ* observation of protein phosphorylation by high-resolution NMR spectroscopy. *Nat. Struct. Mol. Biol.* **15,** 321–329 CrossRef Medline
29. Reimer, U., and Fischer, G. (2002) Local structural changes caused by peptidyl-prolyl cis/trans isomerization in the native state of proteins. *Biophys. Chem.* **96,** 203–212 CrossRef Medline
30. Mitrea, D. M., Grace, C. R., Buljan, M., Yun, M.-K., Pytel, N. J., Satumba, J., Nourse, A., Park, C.-G., Madan Babu, M., White, S. W., and Kriwacki, R. W. (2014) Structural polymorphism in the N-terminal oligomerization domain of NPM1. *Proc. Natl. Acad. Sci. U.S.A.* **111,** 4466–4471 CrossRef Medline
31. Hardie, D. G. (2011) AMP-activated protein kinase: an energy sensor that regulates all aspects of cell function. *Genes Dev.* **25,** 1895–1908 CrossRef Medline
32. Marin, T. L., Gongol, B., Martin, M., King, S. J., Smith, L., Johnson, D. A., Subramaniam, S., Chien, S., and Shyy, J. Y. (2015) Identification of AMP-activated protein kinase targets by a consensus sequence search of the proteome. *BMC Systems Biol.* **9,** 13 CrossRef Medline
33. Safaei, J., Maňuch, J., Gupta, A., Stacho, L., and Pelech, S. (2011) Prediction of 492 human protein kinase substrate specificities. *Proteome Sci.* **9,** S6 CrossRef Medline
34. Johnson, C., Crowther, S., Stafford, M. J., Campbell, D. G., Toth, R., and MacKintosh, C. (2010) Bioinformatic and experimental survey of 14-3-3-binding sites. *Biochem. J.* **427,** 69–78 CrossRef Medline
35. Würtele, M., Jelich-Ottmann, C., Wittinghofer, A., and Oecking, C. (2003) Structural view of a fungal toxin acting on a 14-3-3 regulatory complex. *EMBO J.* **22,** 987–994 CrossRef Medline
36. Trinh, D. L., Scott, D. W., Morin, R. D., Mendez-Lago, M., An, J., Jones, S. J., Mungall, A. J., Zhao, Y., Schein, J., Steidl, C., Connors, J. M., Gascoyne, R. D., and Marra, M. A. (2013) Analysis of FOXO1 mutations in diffuse large B-cell lymphoma. *Blood* **121,** 3666–3674 CrossRef Medline
37. Greer, E. L., Banko, M. R., and Brunet, A. (2009) AMP-activated protein kinase and FoxO transcription factors in dietary restriction-induced longevity. *Ann. N.Y. Acad. Sci.* **1170,** 688–692 CrossRef Medline
38. Bah, A., Vernon, R. M., Siddiqui, Z., Krzeminski, M., Muhandiram, R., Zhao, C., Sonenberg, N., Kay, L. E., and Forman-Kay, J. D. (2015) Folding of an intrinsically disordered protein by phosphorylation as a regulatory switch. *Nature* **519,** 106–109 CrossRef Medline
39. Yang, J., Cron, P., Good, V. M., Thompson, V., Hemmings, B. A., and Barford, D. (2002) Crystal structure of an activated Akt/protein kinase B ternary complex with GSK3-peptide and AMP-PNP. *Nat. Struct. Biol.* **9,** 940–944 CrossRef Medline
40. Gegenbauer, K., Elia, G., Blanco-Fernandez, A., and Smolenski, A. (2012) Regulator of G-protein signaling 18 integrates activating and inhibitory signaling in platelets. *Blood* **119,** 3799–3807 CrossRef Medline
41. Beaven, R., Bastos, R. N., Spanos, C., Romé, P., Cullen, C. F., Rappsilber, J., Giet, R., Goshima, G., and Ohkura, H. (2017) 14-3-3 regulation of Ncd reveals a new mechanism for targeting proteins to the spindle in oocytes. *J. Cell Biol.* **216,** 3029–3039 CrossRef Medline
42. Molzan, M., Schumacher, B., Ottmann, C., Baljuls, A., Polzien, L., Weyand, M., Thiel, P., Rose, R., Rose, M., Kuhenne, P., Kaiser, M., Rapp, U. R., Kuhlmann, J., and Ottmann, C. (2010) Impaired binding of 14-3-3 to C-RAF in Noonan syndrome suggests new approaches in diseases with increased Ras signaling. *Mol. Cell. Biol.* **30,** 4698–4711 CrossRef Medline
43. Dalle Pezze, P., Ruf, S., Sonntag, A. G., Langelaar-Makkinje, M., Hall, P., Heberle, A. M., Razquin Navas, P., van Eunen, K., Tölle, R. C., Schwarz, J. J., Wiese, H., Warscheid, B., Deitersen, J., Stork, B., Fäßler, E., *et al.* (2016) A systems study reveals concurrent activation of AMPK and mTOR by amino acids. *Nat. Commun.* **7,** 13254 CrossRef Medline
44. Leclerc, G. M., Leclerc, G. J., Fu, G., and Barredo, J. C. (2010) AMPK-induced activation of Akt by AICAR is mediated by IGF-1R dependent and independent mechanisms in acute lymphoblastic leukemia. *J. Mol. Signal.* **5,** 15–15 CrossRef Medline
45. Zou, J., Hong, L., Luo, C., Li, Z., Zhu, Y., Huang, T., Zhang, Y., Yuan, H., Hu, Y., Wen, T., Zhuang, W., Cai, B., Zhang, X., Huang, J., and Cheng, J. (2016) Metformin inhibits estrogen-dependent endometrial cancer cell growth by activating the AMPK–FOXO1 signal pathway. *Cancer Sci.* **107,** 1806–1817 CrossRef Medline
46. Ning, Y., Li, Z., and Qiu, Z. (2015) FOXO1 silence aggravates oxidative stress-promoted apoptosis in cardiomyocytes by reducing autophagy. *J. Toxicol. Sci.* **40,** 637–645 CrossRef Medline
47. Studier, F. W. (2005) Protein production by auto-induction in high density shaking cultures. *Protein Expr. Purif.* **41,** 207–234 CrossRef Medline
48. Sivashanmugam, A., Murray, V., Cui, C., Zhang, Y., Wang, J., and Li, Q. (2009) Practical protocols for production of very high yields of recombinant proteins using *Escherichia coli*. *Protein Sci.* **18,** 936–948 CrossRef Medline
49. Kunzelmann, S., and Webb, M. R. (2010) A fluorescent, reagentless biosensor for ADP based on tetramethylrhodamine-labeled ParM. *ACS Chem. Biol.* **5,** 415–425 Medline
50. Vranken, W. F., Boucher, W., Stevens, T. J., Fogh, R. H., Pajon, A., Llinas, M., Ulrich, E. L., Markley, J. L., Ionides, J., and Laue, E. D. (2005) The CCPN data model for NMR spectroscopy: development of a software pipeline. *Proteins* **59,** 687–696 CrossRef Medline
51. Rosenlöw, J., Isaksson, L., Mayzel, M., Lengqvist, J., and Orekhov, V. Y. (2014) Tyrosine phosphorylation within the intrinsically disordered cytosolic domains of the B-cell receptor: an NMR-based structural analysis. *PLoS ONE* **9,** e96199 CrossRef Medline